Chemical Science

ROYAL SOCIETY OF CHEMISTRY

EDGE ARTICLE

View Article Online
View Journal | View Issue

Cite this: *Chem. Sci.*, 2024, **15**, 18608

All publication charges for this article have been paid for by the Royal Society of Chemistry

Non-innocent P-centers in nonbenzenoid polycyclic aromatic molecules with tunable structures and properties†

Can Li,‡[a] Wei Zhou,‡[a] Zhaoxin Liu,‡[a] Rong Gao,[a] Qixi Mi,[a] Zhijun Ning *[a] and Yi Ren *[ab]

Implanting heteroatoms into polycyclic aromatic molecules (PAMs) offers a great opportunity to fine-tune their optoelectronic properties. Herein, we report a new type of nonbenzenoid PAM in which the sp^2 C atoms are replaced by S and P in the azulene moiety. The synthesis harnessed modular P-chemistry and cyclization chemistry, which afforded the first example of P-azulene-based PAMs with isomeric PN- and PC-type structures. Photophysical and theoretical studies revealed that the P-environments have strong impacts on the structures and properties of the P-PAMs. Different from the electronic structure of azulene with strong π conjugation, the PC derivatives maintained effective σ*–π* hyperconjugation in the frontier molecular orbitals *via* the P-centers. In particular, the PC derivative with a P(III)-center showed unexpected room-temperature phosphorescence in solution, which was attributed to the excited-state aromaticity induced structure change at the P-center. Decoration with various aryl groups further modified the photophysical and redox properties in another dimension. Furthermore, bis(triarylamine)-functionalized P-PAMs formed stable radical cations in which the P-environments strongly influenced the mixed-valence state and open-shell characters. As a proof of concept, bis(triarylamine)-functionalized P-PAMs were explored as the hole-transporting layers in perovskite solar cells, and a power conversion efficiency of 14% was achieved. As a new example of nonbenzenoid PAMs with intriguing optoelectronic properties, our P-PAMs are promising building blocks for diverse optoelectronic applications in the future.

Received 31st August 2024
Accepted 7th October 2024

DOI: 10.1039/d4sc05857g

rsc.li/chemical-science

Introduction

Polycyclic aromatic molecules (PAMs) have attracted significant attention in the areas of organic catalysis, bio-imaging/sensing, and organic optoelectronic devices.[1–6] Compared with classical benzenoid PAMs, nonbenzenoid PAMs have recently maintained a unique position in the applications mentioned above.[7–11] Adding or removing sp^2 C atoms in benzenoid PAMs is one popular strategy to build nonbenzenoid PAMs. For example, nonbenzenoid PAMs with five-membered rings have been extensively investigated in the field of organic radical materials, as their open-shell characteristics can be readily activated and tuned.[11–16] Azulene, with a fused five-membered and seven-membered ring, is another classical example of a nonbenzenoid PAM with unique anti-Kasha emission properties, redox characters, and optoelectronic functionalities.[7,17–21]

Replacing the sp^2 C atoms with main-group elements (such as B,[12,22–26] N,[7,27–30] S,[31–34] Si,[7,35] P,[36–41] *etc.*) is another popular strategy to construct nonbenzenoid PAMs with diverse chemical/electronic properties. Phosphorus (P) is a special element among the main-group elements that exhibits rich functionalities, such as oxidation, borylation, alkylation, and metal coordination.[36,37] These functionalities further facilitate efficient σ(σ*)–π(π*) hyperconjugations between the P-centers and π-conjugated backbones, thus greatly enriching its applications in terms of two-photon emission, electron-accepting character, and electrochromic devices. These intriguing functions are not easily accessible to the traditional purely carbon-based PAMs.

Recently, research into P-six-membered PAMs has started to emerge due to the discovery of new synthetic protocols.[41–46] For example, Romero and co-workers recently reported phosphaphenalene derivatives *via* facile cyclization chemistry.[41] In another example, Yamaguchi and co-workers reported new P-xanthene derivatives with excellent near-IR fluorescence imaging properties. Our group also developed a new modular

[a]*School of Physical Science and Technology, ShanghaiTech University, Shanghai 201210, China. E-mail: renyi@shanghaitech.edu.cn; ningzhj@shanghaitech.edu.cn*

[b]*Shanghai Clinical Research and Trial Center, Shanghai, 201210, People's Republic of China*

† Electronic supplementary information (ESI) available. CCDC 2379333–2379336. For ESI and crystallographic data in CIF or other electronic format see DOI: https://doi.org/10.1039/d4sc05857g

‡ These authors contributed equally.

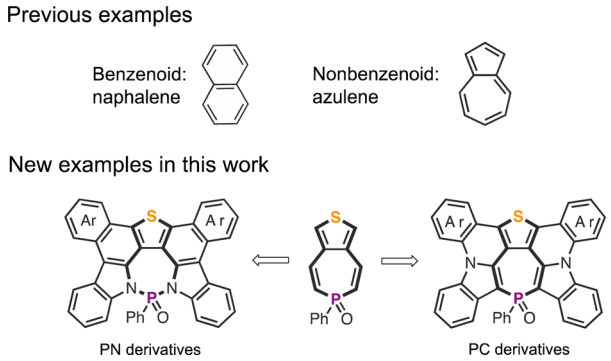

Chart 1 Nonbenzenoid PAMs in previous studies and the new nonbenzenoid P-PAMs (PN and PC derivatives) in this study.

protocol to access highly emissive diazaphosphinines with tunable singlet and triplet emission.[46]

Compared with P-five-/six-membered PAMs, research into P-seven-membered PAMs is still in its infancy, mainly because of their synthetic challenges and/or instability.[47–52] Therefore, it is highly desirable to develop the streamlined protocols that can efficiently construct P-seven-membered PAMs with more complex and rich functionalities. Herein, we report new examples of nonbenzenoid PAMs with S-five-P-seven heterocycles (Chart 1). Leveraging the efficient P-chemistry and cyclization chemistry, the modular synthesis afforded P-PAMs with structural diversity. Distinct structures allowed us to fine-tune the electronic structures and photophysical properties in both the ground and excited state. Further decorating P-PAMs with various aryl substituents systematically modified their photophysical properties, redox behaviors, and radical characteristics. As a proof of concept, P-PAMs with triaryl amine groups were successfully applied as hole-transporting layers in perovskite solar cells.

Results and discussion

The synthesis of the new P-PAMs started with tetrabromothiophene (**1**), which was converted into various 2,5-diaryl thiophene derivatives (**2a,b,c** and **2d,e,f**) *via* Suzuki coupling reactions (Scheme 1(i)). Subsequent Suzuki coupling reactions between **2a,b,c**/**2d,e,f** and 2-(4,4,5,5-tetramethyl-1,3,2-dioxaborolan-2-yl)-1*H*-indole afforded **3a,b,c** and **3d,e,f** in moderate yields. Using P–N and P–C bond formation protocols reported in our previous studies,[46,50,51] we were able to synthesize **4a** (90%), **4b** (93%), **4c** (85%), **5d** (70%), and **5e** (81%) with P-heteropine units.

Unlike **5d** and **5e**, **5f** could not be obtained under similar reaction conditions. Alternatively, we used a synthetic method reported by Masahiro and coworkers with modified conditions, in which activated phenylphosphinic acid was used as the starting reagent (Scheme 1(v)).[53] This method gave **5fO** with a yield of 31%. Oxidation of **4a,b,c** and **5d,e** with excess H_2O_2

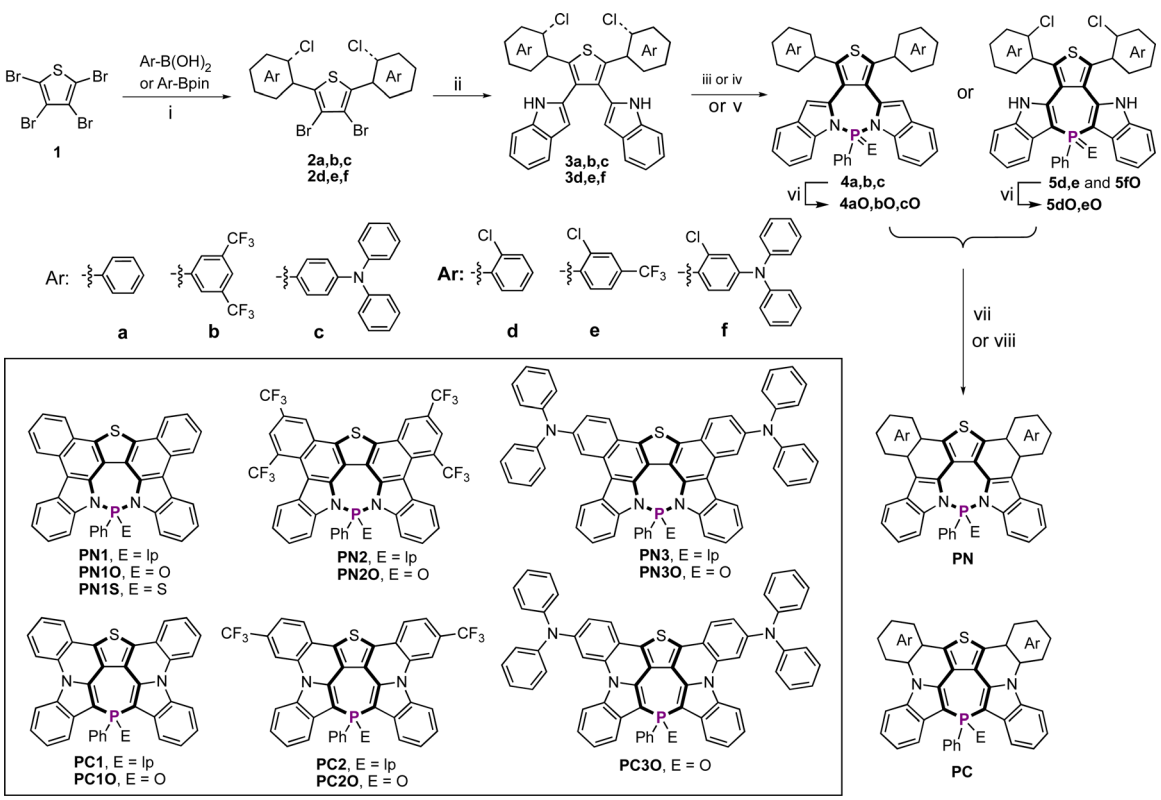

Scheme 1 Synthesis of new P-PAMs with isomeric structures. (i) $Pd(PPh_3)_4$, base, solvent, Δ. (ii) $Pd(OAc)_2$, Ruphos, K_3PO_4, solvent, Δ. (iii) $PhPCl_2$, DBU, acetonitrile. (iv) $PPhCl_2$ (1.3 eqv.), TMSOTf (2.6 eqv.), CH_3CN, −30 °C → 70 °C. (v) PhP(O)H(OH), DMAP, −30 °C → 70 °C. (vi) H_2O_2 (excess), r.t. in DCM. (vii) DDQ, 365 nm LED, dry toluene, r.t. (viii) CuI, K_3PO_4, DMEDA, DMF, 140 °C.

afforded **4aO**/**bO**/**cO** and **5dO**/**5eO** in high yields (Scheme 1(vi)). **4a** was chosen as the representative molecule for the sulfuration of the P-center. After heating with S_8 (10 eqv.) at 140 °C for 10 days, we were able to obtain **4aS** in a yield of 96%.

To further planarize the backbones, photocyclization was applied to **4a**/**b**/**c** and **4aO**/**bO**/**cO**. In previous studies, Scholl reaction (excess oxidants and Lewis acid) and Mallory reaction (*hv*, excess I_2 and propylene oxide) conditions showed limited compatibility with the cyclization of P-PAMs with various P-centers.[38,43,54–56] In our case, the photocyclizations were highly efficient when DDQ was used as the oxidant, giving the PN series in good yields (Scheme 1(vii)). The isomeric counterparts **PC1**/**2** and **PC1**/**2**/**3O** were obtained by applying the intramolecular CuI-catalyzed C–N coupling reaction to **5d**/**e** and **5d**/**e**/**fO** (Scheme 1(viii)). The results showed that the presence of the P(III) and P═O centers did not affect the CuI-catalyzed cyclization. Compared with Pd/Ni-catalyzed cyclizations reported previously,[57,58] the CuI-catalyzed cyclization of P-PAMs has rarely been reported in the literature.

We also tried to synthesize **PC3** with a P(III) center by reducing **PC3O** with $SiHCl_3$. However, the easy oxidation of **PC3** prevented us from obtaining the pure product during the purification. The synthesis of the new P-PAMs demonstrated a highly modular protocol to access new nonbenzenoid PAMs with the great structural tunability. Due to their large aromatic structures, some of the products exhibited low solubilities in typical organic solvents. The detailed synthesis and characterizations are provided in the ESI.†

We were able to obtain suitable single crystals of **PN1S**, **PN2O**, **PN3O**, **PC1O**, and **PC3O** for single-crystal X-ray diffraction experiments (Fig. 1 and Table S1†). The single-crystal structure of **PN2O** contains a disordered solvent, which resulted in a low crystal data quality (Fig. S9†). In the crystal structures of **PN1S** and **PN3O**, the fused polycyclic aromatic structures induced planar backbones. However, the P-centers were significantly twisted out of the central heteropine plane (Fig. 1a and b), with distances between the P-center and the heteropine plane of 0.9 Å for **PN1S** and 0.7 Å for **PN3O**, respectively. These results differ from those for previous six-membered diazaphosphinines, in which the central six-membered P-ring showed high planarity.[46] The P–N bond lengths of **PN1S** (1.70 Å) and **PN3O** (1.69 Å) are similar to those of previous diazaphosphepines.[46,50,51]

Compared with the PN derivatives, **PC1O** and **PC3O** showed more planarized P-heteropine planes (Fig. 1c and d). The distances between their P-centers and the heteropine planes are significantly shorter (**PC1O:** 0.2 Å and **PC3O:** 0.01 Å) compared with those of **PN1S** and **PN3O**. The P–C bond lengths of **PC1O** (1.77 Å) and **PC3O** (1.77 Å) are at shorter end of the range for P–C bonds (1.77–1.81 Å) reported in previous P-heteropines, which suggested a strong π-delocalization between the P-center and heteropine backbone.[47–50] Furthermore, strong intermolecular π–π interactions were observed in these crystal structures. For example, **PN1S** and **PC3O** showed dimeric π–π interaction (Fig. S1 and S7†), whereas **PN3O** and **PC1O** showed long-range intermolecular π–π interactions (Fig. S3 and S5†).

We conducted UV-vis and fluorescence spectroscopy experiments on new P-PAMs (Fig. 2a, b and S10–S12†). Due to their rigid structures, both the PN and PC series exhibited small Stokes shifts. Consistently, the absorption and emission spectra showed the typical vibronic structures of rigid aromatic molecules. Upon decoration with electron-withdrawing and electron-donating aryl groups, the PN and PC series showed tunable absorption and emission.

The absorption and emission spectra of the PC series were systematically red-shifted compared to those of the PN series (Fig. 2a and b). It is rationalized that the strong π-conjugation of the PC series is responsible for the smaller LUMO–HOMO gaps,

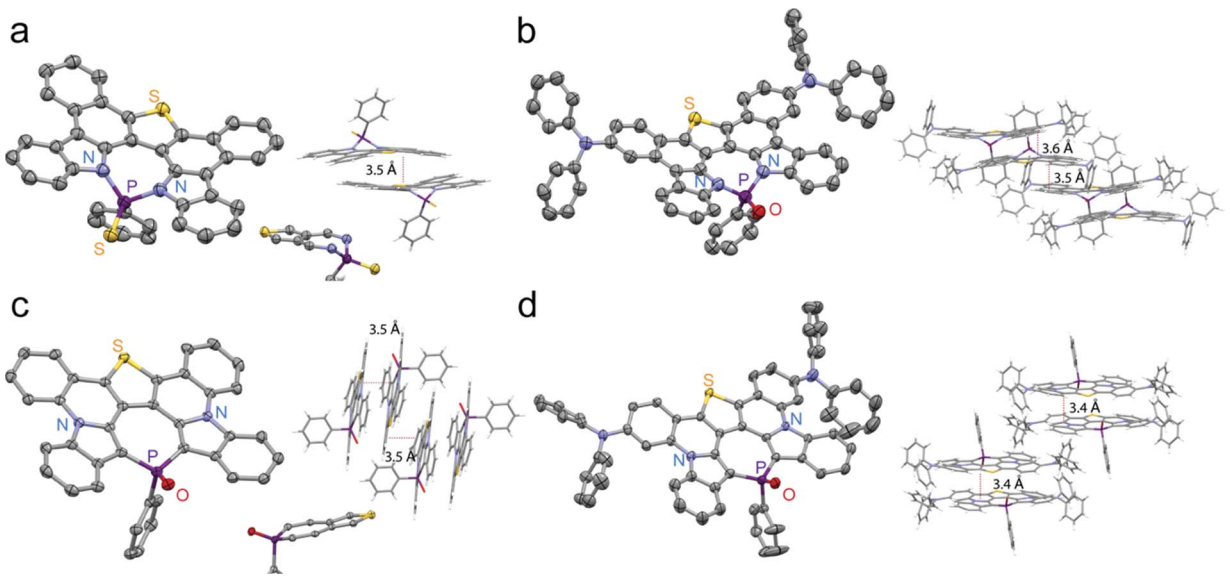

Fig. 1 Single crystal structures of (a) **PN1S**, (b) **PN3O**, (c) **PC1O**, and (d) **PC3O** (thermal ellipsoids are shown at 50% probability level; hydrogen atoms are omitted for clarity).

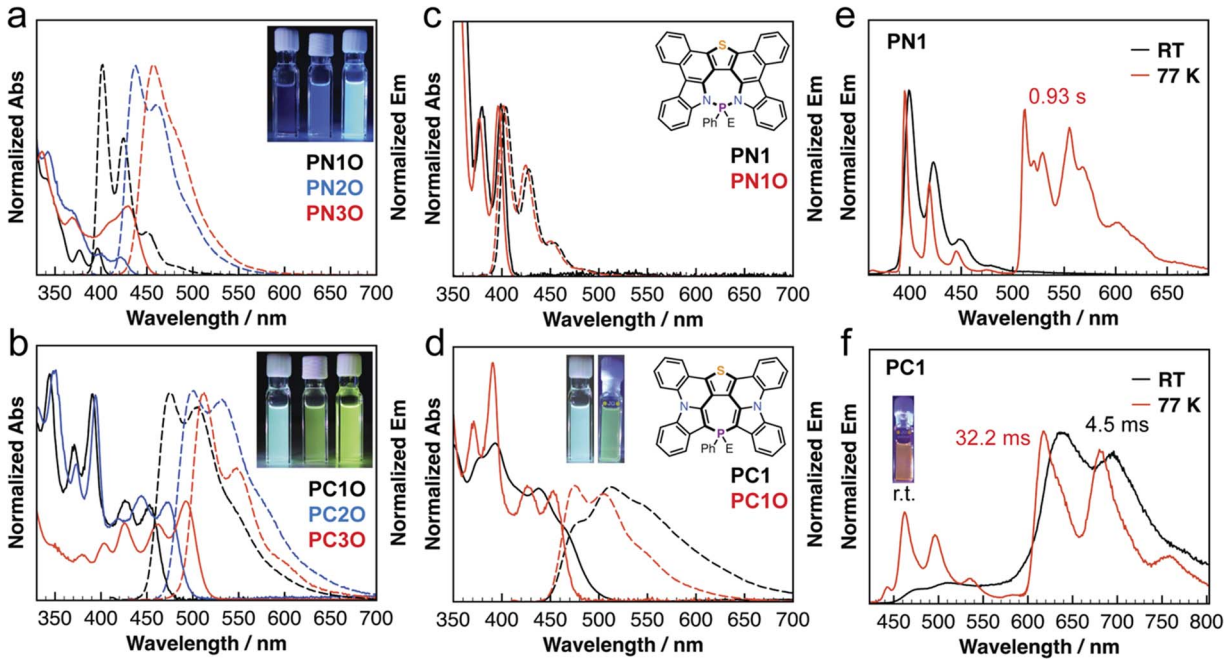

Fig. 2 (a and b) Absorption and emission spectra of PN and PC in CH_2Cl_2. (c and d) Absorption and emission spectra of the **PN1** series and **PC1** series in CH_2Cl_2. (e and f) Low-temperature emission spectra of **PN1** and **PC1** in 2Me-THF at 77 K.

thus resulting in the red-shifted spectra (*vide infra*). The results highlighted the distinct structure impacts on the photophysical properties of the P-PAMs. Furthermore, **PN1**, **PN1O** and **PN1S** exhibited similar absorption and emission spectra (Fig. 2c and S10†), suggesting that the changes in the P-chemistry scarcely modified the optical bandgaps. This is not true for the PC series. As shown in Fig. 2d, **PC1O** (λ_{abs} = 453 nm and λ_{em} = 475 nm) with a P═O center exhibited blue-shifted absorption and emission spectra compared with those of **P1C** (λ_{abs} = 463 nm and λ_{em} = 511 nm) with a P(III) center. The emission spectrum of **PC1** is also broader than that of **PC1O**. The photophysical characteristics of **PC1** were unexpected, since rigid P-PAMs with a P═O center have generally exhibited red-shifted absorption and emission spectra compared with those with a P(III) center in previous studies.[9,35] It is rationalized that **P1C** with a flexible P-center underwent a significant structure change in the excited state (*vide infra*), thus leading to the red-shifted emission. Although heteropines are well-known for their conformational dynamics in both the S_0 and S_1 states,[47–52,59–61] the conformational dynamics of fused heteropine-PAMs have not been addressed in the literature.

The PN series consistently exhibited lower photoluminescence quantum yields (PLQYs; for example, **PN1O**: 11% and **PN2O**: 14%) compared with the PC series (PLQYs: 25% for **PC1O**, 30% for **PC2O**), except for those with triaryl amine groups (83% for **PN3O**, 81% for **PN3**). We further conducted low-temperature fluorescence spectroscopy experiments on the PN and PC series in 2Me-THF solution (Fig. 2e, f, S13 and S14†). In addition to the fluorescence emission signals, we also observed phosphorescence emission signals at 77 K. The phosphorescence signals of **PN1**, **PN1O**, **PN1S**, **PN2**, and **PN2O** were more pronounced than the fluorescence signals (Fig. S13 and S14†). Consistently, the phosphorescence lifetimes of PN series are longer than those of PC series (Table 1). These results suggested that the low PLQYs of the PN series are probably due to the strong intersystem crossing.

Unexpectedly, **PC1** exhibited a low-energy red emission in 2Me-THF solution at room temperature (Fig. 2f). The triplet-state nature of the emission was further confirmed by the long lifetime (0.45 ms) (Fig. S38†). Such observations were not made for **PN1** (Fig. 2e). There are only a few molecules that show room-temperature phosphorescence in solution.[62–64] To the best

Table 1 Photophysical data of P-PAMs[a]

Compound[b]	λ_{abs}[b] [nm]	λ_{em}[c] [nm]	ϕ_{PL}[d] [%]	τ_{FL}[e] [ns]	τ_{Ph}[f] [s]
PN1	399	404	11	1.50	0.93
PN1O	396	402	11	1.46	0.98
PN1S	398	403	7	0.88	0.95
PN2	420	438	10	1.41	0.41
PN2O	421	441	14	1.27	0.40
PN3	428	453	81	1.51	0.51
PN3O	430	458	83	1.61	0.51
PC1	438	511	NA[g]	0.61	0.03
	463 (sh)				
PC1O	453	475	25	0.74	0.09
PC2	454	535	1	1.16	0.04
PC2O	473	501	30	1.01	0.05
PC3O	492	512	53	0.48	0.04

[a] Measured in CH_2Cl_2. [b] Absorption maximum of the lowest absorption band. [c] Emission maximum. [d] Measured by the calibrated integrating sphere. [e] Measured in DCM at room temperature. [f] Measured in 2Me-THF at 77 K. [g] Not detectable by the calibrated integrating sphere.

of our knowledge, there have been no reports of P-heteropines showing room-temperature phosphorescence in solution. Previous studies showed that the nonbonding electron lone pair of heteroatom groups effectively enhanced the spin–orbit coupling (SOC), thus promoting the triplet emission.[65–67] The structure change of **PC1** likely enhanced the SOC, further leading to the unexpected room-temperature phosphorescence. At 77 K, at which the conformational changes of **PC1** were suppressed, an enhanced fluorescence signal was observed (Fig. 2f).

To shed light on the distinct photophysical characteristics of the PNO and PCO series, we conducted theoretical studies using density functional theory (DFT) and time-dependent (TD)-DFT (see the details in the ESI†). Fig. 3a shows the frontier molecular orbitals (FMOs) of the PN and PC series. The presence of electron-withdrawing substituents mainly lowers the LUMOs, while the presence of electron-donating substituents strongly raised the HOMOs. Consequently, the presence of electron-withdrawing and electron-donating substituents resulted in the lower HOMO–LUMO bandgaps ($\Delta E_{\mathrm{HOMO-LUMO}}$) and S_0–S_1 transition energy in both the PNO and PCO series (Table S2†). Furthermore, the PC series exhibited lower $\Delta E_{\mathrm{HOMO-LUMO}}$ values and S_0–S_1 transition energy compared with the PN series (Fig. 3a and S2†), which are consistent with the photophysical characteristics described in the previous section.

Different from those of the PNO series, the HOMOs of the central S-five-P-seven moiety clearly show π-bond character in the PCO series, and are very similar to HOMOs of azulene (A, Fig. 3b). However, the LUMOs of the central S-five-P-seven moiety in the PCO series are different from those of azulene. We further conducted natural bond orbital (NBO) analysis, which can provide the second-order perturbation energy (E) associated with the stabilization of hyperconjugation in P-PAMs.[68,69] For **PC1O**, the results suggested a negative hyperconjugation ($E = 3.09$ kcal mol^{-1}) between the σ*-orbital of the P–C/O bonds and the π* orbitals of heterocycle backbone. These results are in line with the lower-energy bandgaps of the PCO derivatives. Similar results are also observed in the parent PO-azulene (C, Fig. 3b).

We conducted excited-state studies to examine the unexpected room-temperature phosphorescence in solution. As shown in Fig. 3c, **PC1** underwent a significant structure change in the S_1 state, in which the sum of the three C–P–C bond angles (327°) increased in the S_1 state (*cf.* 308° in S_0). The results suggested that the P(III)-center adopted a more planar geometry in the excited state. Furthermore, the lone-pair electrons of **PC1**

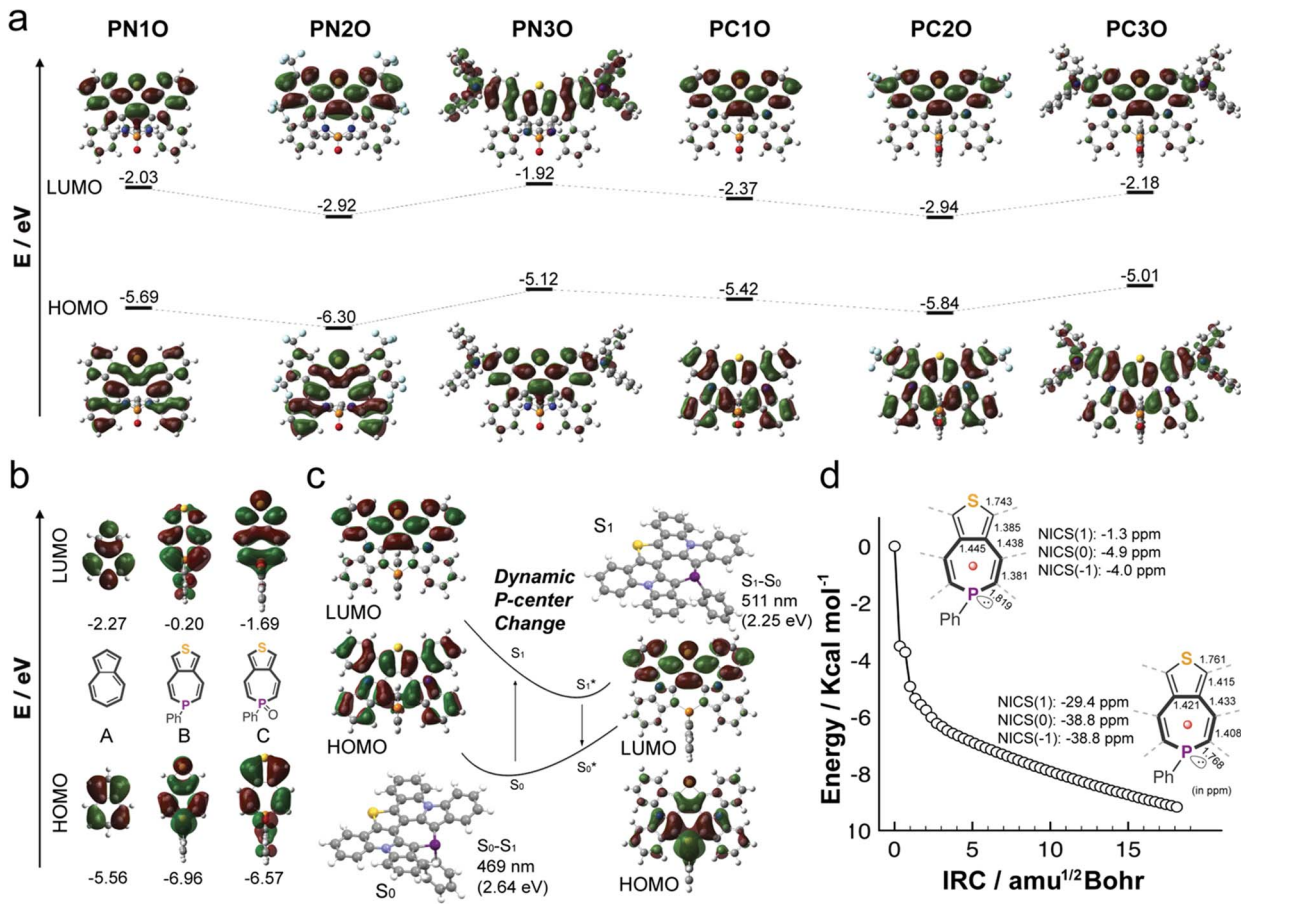

Fig. 3 (a and b) FMOs of the PNO series, PCO series, azulene, and heteroatom-azulenes. (c) Optimized structures and FMOs of **PC1** in S_0 and S_1 (TD-DFT calculated at the B3LYP/6-311+G(d,p) level). (d) Intrinsic reaction coordinate of **PC1** in S_1 (B3LYP/6-311G(d,p) level). Insert: NICS values in S_0 and T_1 (calculated at the (U)B3LYP/6-311+G(d,p) level in a vacuum).

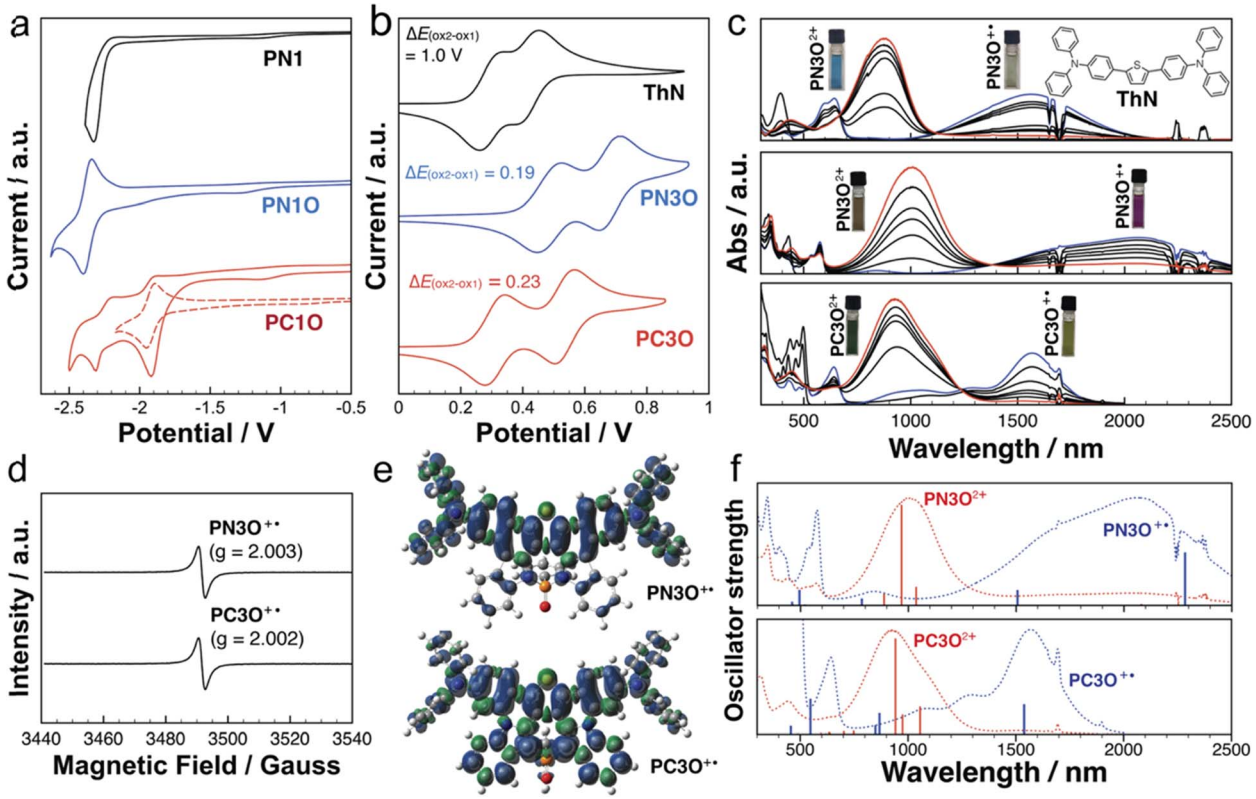

Fig. 4 (a and b) Cyclic voltammograms of new P-PAMs. (c) UV-vis-NIR spectra of ThN, **PN3O** and **PC3O** (1×10^{-5} M) with different amounts of $AgSbF_6$ in DCM. (d) Solid-state EPR spectra of **PN3O** and **PC3O** monocations. (e) Spin density of **PN3O** and **PC3O** radical cations calculated at CAM-UB3LYP/6-311+G(d,p) in a vacuum. (f) Theoretical calculated optical transitions of **PN3O** and **PC3O** cations calculated at (CAM)-(U)B3LYP/6-311+G(d,p) in a vacuum.

displayed a strong contribution to the HOMO of the S_1 state. This observation differs from that for P-azulene, in which the lone-pair electrons display a strong contribution to HOMO of the S_0 state (B, Fig. 3b). A similar structure change is not observed for **PN1** in the excited state (Fig. S40†). We further conducted intrinsic reaction coordinate (IRC) calculations (Fig. 3d) to visualize the excited state evolution of **PC1** between the initial S_0 structure and the final S_1 structure (see the details in the ESI†). The IRC results showed that P-center planarization occurred downhill, which supported the thermodynamically favorable structure of **PC1** in S_1.

To probe the driving force for the planarization, we conducted nucleus-independent chemical shift (NICS) calculations of the central heteropine in **PC1**. According to Baird's rule, conjugated rings with 4n π electrons are aromatic in T_1, which was further demonstrated to be true for the rings in S_1.[70] NICS for S_1, which requires a multideterminant wavefunction, is more complicated. Due to the limitations of computational approaches at the current stage, we instead performed NICS calculations at the T_1 state, which were used to evaluate the excited state aromaticity in previous studies.[71] As we expected, the large negative NICS values (in ppm) implied that the aromaticity gain is likely the driving force for the excited-state planarization (Fig. 3d).

Although previous studies showed that N-heteropines[72] and As-heteropines[59] underwent excited-state Baird's aromaticity-induced planarization at the As and N centers, similar excited-state planarization of the P-center of heterocycles has not been reported in the literature. In our case, we hypothesized that the planarization of the P-center was more energetically favorable than the change of the fused π-conjugated backbone of **PC1** in S_1.

Cyclic voltammetry (CV) experiments were conducted to reveal the redox characteristics of the new P-PAMs (Fig. 4a and S41†). Due to their limited solubilities, **PC1**, **PC2**, and **PC2O** were not subjected to the CV experiments. Compared with **PN1**, **PN1O** exhibited a more positive reduction potential, likely due to the presence of the strong electron-accepting P═O center. In the PC series, **PC1O** exhibited two reduction potentials. Moreover, the first reversible reduction potential is lower than that of **PN1O**. Based on the theoretical studies, the stronger electron-accepting ability of **PC1O** is attributed to the σ*–π* hyperconjugation.

When the strong electron-donating bis(triarylamine) substituents were installed, **PN3**, **PN3O**, and **PC3O** exhibited two reversible oxidation potentials (Fig. 4b). With the electron-accepting P═O group, the oxidation potentials of **PN3O** (E_{ox1} = 0.49 V, E_{ox2} = 0.68 V) are slightly higher than those of **PN3** (E_{ox1} = 0.45 V, E_{ox2} = 0.65 V). **PC3O** (E_{ox1} = 0.31 V, E_{ox2} = 0.54 V)

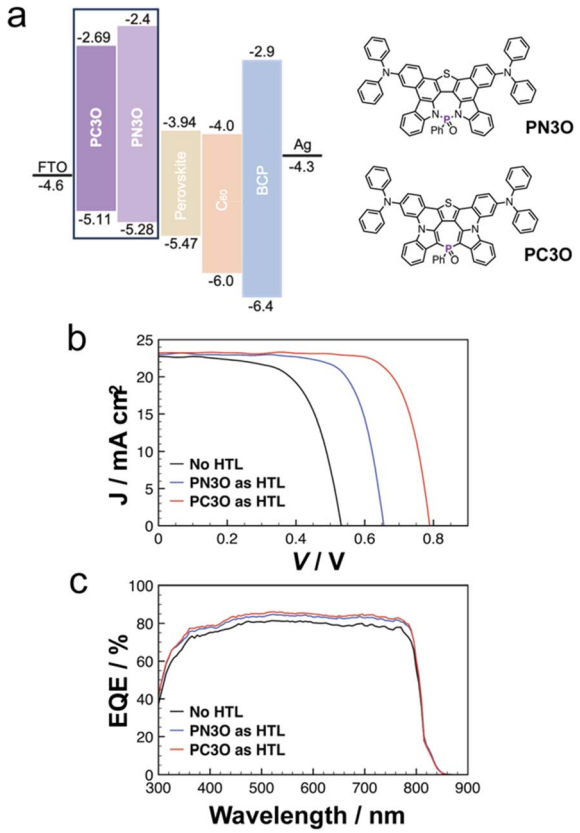

Fig. 5 (a) Device structure using PN3O and PC3O as the HTLs. (b) Density–voltage curves and (c) external quantum efficiency curves of the devices without HTL and with HTLs.

exhibited two lower oxidation potentials than both **PN3** and **PN3O**, suggesting its easier oxidation character. Both **PN3** ($E_{ox2-ox1} = 0.20$ V) and **PN3O** ($E_{ox2-ox1} = 0.19$ V) exhibited larger peak separations compared with **M** ($E_{ox2-ox1} = 0.1$ V), which implied a stronger electronic communication of the bis(triarylamine) groups in **PN3** and **PN3O**. The peak separation was further enlarged for **PC3O** ($\Delta E_{ox2-ox1} = 0.23$ V). The results implied that changing the chemical structure of the heteropine ring significantly influenced the electronic communication of the bis(triarylamine) groups, with **PC3O** maintaining the strongest electronic communication in the current study.

The stable and reversible oxidation character of **PN3**, **PN3O**, and **PC3O** further allowed us to conduct UV-vis-NIR absorption spectroscopy experiments under the different oxidation states (Fig. 4c and d). Upon the addition of $AgSbF_6$ as the oxidation reagent, both **PN3O** and **PC3O** showed a two-step oxidation process. In the first process, new peaks at 2000 nm and 1570 nm were observed for **PN3O** and **PC3O**, respectively. The low-energy transitions were rationalized to the intervalence charge transfer (IVCT) bands, which are characteristic of mixed-valence states in bis(triarylamine) systems.[30,73] Electron paramagnetic resonance (EPR) spectroscopy experiments further revealed a featureless band (Fig. 4d), thus supporting the open-shell character of the **PN3O** and **PC3O** monocations. The theoretical studies of the radical cations not only confirmed the lowest transition (2078 nm for $\mathbf{PN3O}^{+\cdot}$ and 1439 nm for $\mathbf{PC3O}^{+\cdot}$), but also revealed the different spin densities (Fig. 4e and f). Compared with $\mathbf{PN3O}^{+\cdot}$, $\mathbf{PC3O}^{+\cdot}$ showed a broader spin distribution spread over the whole molecular backbone. Particularly, the P-center (spin density: 0.04) of $\mathbf{PC3O}^{+\cdot}$ showed a higher spin density compared with that of $\mathbf{PN3O}^{+\cdot}$ (spin density: 0.001). These results suggested that the P-center of $\mathbf{PC3O}^{+\cdot}$ has a strong impact on the mixed-valence state. Further addition of $AgSbF_6$ converted **PN3O** and **PC3O** to the second stage, in which new peaks at 1000 nm for **PN3O** and 920 nm for **PC3O** emerged. The results implied that both **PN3O** and **PC3O** underwent the transition from the open-shell monocations to the closed-shell quinoid dications, which was supported by the theoretical studies (Fig. 4f).

Previous studies revealed that triaryl amines containing PAMs are promising candidates as hole-transporting layers (HTL) in perovskite solar cells (PSCs). Furthermore, P═O functional groups were also demonstrated to be beneficial for the interface coordination and passivation of PSCs.[74] Therefore, **PN3O** and **PC3O** were explored as new HTLs in inverted PSCs (Fig. 5, and see the details in the ESI†).

We first fabricated the PSC devices in an HTL-free configuration (Fig. 5b and c). From the current density–voltage (J–V) curves of the device, the HTM-free device showed a low power conversion efficiency (PCE) of 7.68%. Then, **PN3O** was integrated as an HTM into the device, which showed an improved V_{oc} (0.65 V) and FF (73%). The results indicated that **PN3O** played a better role in hole extraction and hole transport. We further used **PC3O** as the HTL in the PSCs. The PCE further reached up to 14.0% with a V_{oc} of 0.79 V, FF of 75%, and short-circuit current density (J_{sc}) of 23.25 mA cm^{-2}. Based on the CV experiments (Fig. 5a), the improved V_{oc} can be attributed to the more suitable HOMO energy level of **PC3O** (−5.11 eV) compared with that of **PN3O** (−5.28 eV).

Conclusions

Herein, we have reported a new family of nonbenzenoid PAMs containing S-five-P-seven heterocycles. The selective P-chemistry and cyclization chemistry are modular to afford the target molecules with isomeric PN and PC structures. The distinct P-environments endowed the systems with intriguing photophysical, redox, and radical characteristics. Compared with the PN derivatives, the PC derivatives showed more planar S-five-P-seven heterocycles. Different from the electronic structure of azulene, the S-five-P-seven heterocycles of the PC derivatives maintained the effective σ*–π* hyperconjugation *via* the P-centers. This was not the case for PN derivatives. Experimental and theoretical results suggested that the PC derivative with a P(III) center underwent a structure planarization in S_1, thus resulting in the unexpected room-temperature phosphorescence in solution. After decoration with two triarylamine groups, the P-PAMs readily formed stable radical cations, in which the PC derivative exhibited a stronger mixed-valence state and more delocalized radical density. As a proof of concept, bis(triarylamine) functionalized P-PAMs were successfully used as the HTLs in perovskite solar cells, which showed the

promising PCE of 14%. Overall, our work provides a new design strategy for nonbenzenoid PAMs with intriguing optoelectronic properties.

Data availability

The data supporting this article have been included as part of the ESI.†

Author contributions

The manuscript was written through contributions of all authors.

Conflicts of interest

There are no conflicts to declare.

Acknowledgements

This research was financially supported by ShanghaiTech University start-up funding. YR also acknowledges the support from Shanghai Clinical Research and Trial Center, Analytical Instrumentation Center (SPST-AIC10112914), SPST, and the HPC Platform of ShanghaiTech University for providing resources and computing time. The authors cordially thank Shuya Wen for the assistant of the single-crystal X-ray measurements.

Notes and references

1 J. Corrigan, J. Yeow, P. Judzewitsch, J. Xu and C. Boyer, *Angew. Chem., Int. Ed.*, 2019, **58**, 5170–5189.
2 J. E. Anthony, *Angew. Chem., Int. Ed.*, 2008, **47**, 452–483.
3 A. Mishra and P. Bäuerle, *Angew. Chem., Int. Ed.*, 2012, **51**, 2020–2067.
4 M. Ball, Y. Zhou, Y. Wu, C. Schenck, F. Ng, M. Steigerwald, S. X. Xiao and C. Nuckolls, *Acc. Chem. Res.*, 2015, **48**, 267–276.
5 H. Xin, B. Hou and X. Gao, *Acc. Chem. Res.*, 2021, **54**, 1737–1753.
6 S. H. Pun and Q. Miao, *Acc. Chem. Res.*, 2018, **51**, 1630–1642.
7 M. Hirai, N. Tanaka, M. Sakai and S. Yamaguchi, *Chem. Rev.*, 2019, **119**, 8291–8331.
8 C. Chen, J.-Y. Zhang, X.-Y. Wang and J. Pei, *Chem. Mater.*, 2023, **35**, 10277–10294.
9 Chaolumen, I. A. Stepek, K. E. Yamada, H. Ito and K. Itami, *Angew. Chem., Int. Ed.*, 2021, **60**, 23508–23532.
10 J. Liu, S. Mishra, C. A. Pignedoli, D. Passerone, J. I. Urgel, A. Fabrizio, T. G. Lohr, J. Ma, H. Komber, M. Baumgarten, C. Corminboeuf, R. Berger, P. Ruffieux, K. Müllen, R. Fasel and X. Feng, *J. Am. Chem. Soc.*, 2019, **141**, 12011–12020.
11 H. Koki, R. Kishi, M. Nakano, D. Shiomi, K. Sato, T. Takui, A. Konishi and M. Yasuda, *J. Am. Chem. Soc.*, 2022, **144**, 3370–3375.
12 M. Mamada, M. Hayakawa, J. Ochi and T. Hatakeyama, *Chem. Soc. Rev.*, 2024, **53**, 1624–1692.
13 C. K. Frederickson, L. N. Zakharov and M. M. Haley, *J. Am. Chem. Soc.*, 2016, **138**, 16827–16838.
14 B. Prajapati, M. D. Ambhore, D.-K. Dang, P. J. Chmielewski, T. Lis, C. J. Góme-García, P. M. Zimmerman and M. Sępień, *Nat. Chem.*, 2023, **15**, 1541–1548.
15 A. Shimizu, R. Kishi, M. Nakano, D. Shiomi, K. Sato, T. Takui, I. Hisaki, M. Miyata and Y. Tobe, *Angew. Chem., Int. Ed.*, 2013, **52**, 6076–6079.
16 P. Cai, X.-Y. Chen, J. Cao, L. Ruppenthal, J. M. Gottfried, K. Müllen and X.-Y. Wang, *J. Am. Chem. Soc.*, 2021, **143**, 5314–5318.
17 Y. Zhou, G. Baryshnikov, X. Li, M. Zhu, H. Ågren and L. Zhu, *Chem. Mater.*, 2018, **30**, 8008–8016.
18 D. Dunlop, L. Ludvíkova, A. Banerjee, H. Ottosson and T. Slanina, *J. Am. Chem. Soc.*, 2023, **145**, 21569–21575.
19 Y. Yamaguchi, M. Takubo, K. Ogawa, K. Nakayama, T. Koganezawa and H. Katagiri, *J. Am. Chem. Soc.*, 2016, **138**, 11335–11343.
20 E. Amir, R. J. Amir, L. M. Campos and C. J. Hawker, *J. Am. Chem. Soc.*, 2011, **133**, 10046–10049.
21 S. Wang, M. Tang, L. Wu, L. Bian, L. Jiang, J. Liu, Z.-B. Tang, Y. Liang and Z. Liu, *Angew. Chem., Int. Ed.*, 2022, **61**, e202205658.
22 K. K. Hollister, A. Molino, G. Breiner, J. E. Walley, K. E. Wentz, A. M. Conley, D. A. Dickie, D. J. D. Wilson and R. J. Hilliard Jr, *J. Am. Chem. Soc.*, 2022, **144**, 590–598.
23 T. Ma, J. Dong and D.-T. Yang, *Chem. Commun.*, 2023, **59**, 13679–13689.
24 M. Crumbach, J. Bachmann, L. Fritze, A. Helbig, I. Krummenacher, H. Braunschweig and H. Helten, *Angew. Chem., Int. Ed.*, 2021, **60**, 9290–9295.
25 M. Metzler, M. A. Virovets, H.-W. Lerner and M. Wagner, *J. Am. Chem. Soc.*, 2023, **145**, 23824–23831.
26 J. Wang, A. Zheng, Y. Xiang and J. Liu, *J. Am. Chem. Soc.*, 2023, **145**, 14912–14921.
27 S. Ito, Y. Tokimaru and K. Nozaki, *Angew. Chem., Int. Ed.*, 2015, **54**, 7256–7260.
28 S. Mishra, M. Krzeszewski, C. A. Pignedoli, P. Ruffieux, R. Fasel and D. T. Gryko, *Nat. Commun.*, 2018, **9**, 1714.
29 S. Hayakawa, A. Kawasaki, Y. Hong, D. Uraguchi, T. Ooi, D. Kim, T. Akutagawa, N. Fukui and H. Shinokubo, *J. Am. Chem. Soc.*, 2019, **141**, 19807–19816.
30 G. Tan and X. Wang, *Acc. Chem. Res.*, 2017, **50**, 1997–2006.
31 T. Jin, L. Kunze, S. Breumaier, M. Bolte, H.-W. Lerner, F. Jäkle, R. F. Winter, M. Braun, J.-M. Mewes and M. Wagner, *J. Am. Chem. Soc.*, 2022, **144**, 13704–13716.
32 W. Wang, F. Hanindita, Y. Tanaka, Y. Kotaro Ochiai, H. Sato, Y. Li, T. Yasuda and S. Ito, *Angew. Chem., Int. Ed.*, 2023, **62**, e202218176.
33 S. Tang, L. Zhang, H. Ruan, Y. Zhao and X. Wang, *J. Am. Chem. Soc.*, 2020, **142**, 7340–7344.
34 S. Takahashi, M. Murai, Y. Hattori, S. Seki, T. Yanai and S. Yamaguchi, *J. Am. Chem. Soc.*, 2024, **146**, 22642–22649.
35 M. Murai, M. Abe, S. Ogi and S. Yamaguchi, *J. Am. Chem. Soc.*, 2022, **144**, 20385–20393.

36 R. Deka, M. A. Ansari, S. Chattopadhyay, R. Lomoth, A. Thapper and A. Orthaber, *Angew. Chem., Int. Ed.*, 2024, e202406076.
37 N. Asok, J. R. Gaffen and T. Baumgartner, *Acc. Chem. Res.*, 2023, **56**, 536–547.
38 P.-A. Bouit, A. Escande, R. Szűcd, D. Szieberth, C. Lescop, L. Nyulászi, M. Hissler and R. Réau, *J. Am. Chem. Soc.*, 2012, **134**, 6524–6527.
39 T. Delouche, E. Caytan, M. Cordier, T. Roisnel, G. Taupier, Y. Molard, N. Vanthuyne, B. L. Guennic, M. Hissler, D. Jacquemin and P.-A. Bouit, *Angew. Chem., Int. Ed.*, 2022, **61**, e202205548.
40 N. Hashimoto, R. Y. Umano, S. Nakamura, S. Mori, H. Ohta, Y. Watanabe and M. Hayashi, *J. Am. Chem. Soc.*, 2018, **140**, 2046–2049.
41 C. Romero-Nieto, A. López-Andarias, C. Egler-Lucas, F. Gebert, J.-R. Neus and O. Pilgram, *Angew. Chem., Int. Ed.*, 2015, **54**, 15872–15875.
42 P. Hindenberg, M. Bush, A. Paul, M. Bernhardt, P. Gemessy, F. Rominger and C. Romero-Nieto, *Angew. Chem., Int. Ed.*, 2018, **57**, 15157–15161.
43 J. D. R. Asherl, C. Neiβ, A. Vogel, J. Graf, F. Rominger, T. Oeser, F. Hampel, A. Görling and M. Kivala, *Chem.–Eur. J.*, 2020, **26**, 13157–13162.
44 L. Xu, D. Wu, W. Lv, Y. Xiang, Y. Liu, Y. Tao, J. Yin, M. Qian, P. Li, L. Zhang, S. Chen, O. F. Mohammed, O. M. Bakr, Z. Duan, R. Chen and W. Huang, *Adv. Mater.*, 2022, **34**, 2107111.
45 M. Grzybowski, M. Taki, K. Senda, Y. Sato, T. Ariyoshi, Y. Okada, R. Kawakami, T. Imamura and S. Yamaguchi, *Angew. Chem., Int. Ed.*, 2018, **57**, 10137–10141.
46 Z. Yang, C. Li, C. Liu, X. Li, N. Yu and Y. Ren, *Angew. Chem., Int. Ed.*, 2022, **61**, e202212844.
47 H. Jansen, J. C. Slootweg and K. Lammertsma, *Beilstein J. Org. Chem.*, 2011, **7**, 1713–1721.
48 K. Padberg, J. D. R. Ascherl, F. Hampel and M. Kivala, *Chem.–Eur. J.*, 2020, **26**, 3474–3478.
49 T. Delouche, A. Mocanu, T. Roisnel, R. Szűcs, E. Jacques, Z. Benkő, L. Nyulászi, P.-A. Bouit and M. Hissler, *Org. Lett.*, 2019, **21**, 802–806.
50 Z. Yang, X. Li, K. Yang, Z. Zhang, Y. Wang, N. Yu, T. Baumgartner and Y. Ren, *Org. Lett.*, 2022, **24**, 2045–2049.
51 Y. Ren, M. Sezen, F. Gao, F. Jäkle and Y.-L. Loo, *Chem. Sci.*, 2016, **7**, 4211–4219.
52 K. Andoh, M. Murai, P.-A. Bouit, M. Hissler and S. Yamaguchi, *Angew. Chem., Int. Ed.*, 2024, e202410204.
53 K. Nishimura, K. Hirano and M. Miura, *Org. Lett.*, 2020, **22**, 3185–3189.
54 M. Grzybowski, K. Skonieczny, H. Butenschön and D. T. Gryko, *Angew. Chem., Int. Ed.*, 2013, **52**, 9900–9930.
55 K. B. Jørgensen, *Molecules*, 2010, **15**, 4334–4358.
56 O. Fadhel, D. Szieberth, V. Deborde, C. Lescop, L. Nyulászi, M. Hissler and R. Réau, *Chem.–Eur. J.*, 2009, **15**, 4914–4924.
57 T. Delouche, R. Mokrai, T. Roisnel, D. Tondelier, B. Geffroy, L. Nyulászi, Z. Benkö, M. Hissler and P.-A. Bouit, *Chem.–Eur. J.*, 2020, **26**, 1856–1863.
58 Y. Kuninobu, T. Yoshida and K. Takai, *J. Org. Chem.*, 2011, **76**, 7370–7376.
59 I. Kawashima, H. Imoto, M. Ishida, H. Furuta, S. Yamamto, M. Mitsuishi, S. Ianaka, T. Fujii and K. Naka, *Angew. Chem., Int. Ed.*, 2019, **131**, 11812–11816.
60 D. Shukla and P. Wan, *J. Am. Chem. Soc.*, 1993, **115**, 2990–2991.
61 R. Kotani, L. Liu, P. Kumar, H. Kuramochi, T. Tahara, P. Liu, A. Osuka, P. B. Karadakov and S. Saito, *J. Am. Chem. Soc.*, 2020, **142**, 14985–14992.
62 J. Xu, A. Takai, Y. Kobayashi and M. Takeuchi, *Chem. Commun.*, 2013, **49**, 8447–8449.
63 H. Shu, J. Rao, J. Chen, X. Wang, X. Wu, H. Tian, H. Tong and L. Wang, *J. Mater. Chem. C*, 2020, **8**, 14360–14364.
64 A. Lv, W. Ye, X. Jiang, N. Gan, H. Shi, W. Yao, H. Ma, Z. An and W. Huang, *J. Phys. Chem. Lett.*, 2019, **10**, 1037–1042.
65 B. Valeur and M. N. Serberan-Santos, *Molecular Fluorescence: Principles and Applications*, Wiley-VCH, Weinheim, Germany, 2nd edn, 2012.
66 Y. Tao, R. Chen, H. Li, J. Yuan, Y. Wan, H. Jiang, C. Chen, Y. Si, C. Zheng, B. Yang, G. Xing and W. Huang, *Adv. Mater.*, 2018, **30**, 1803856.
67 Z. An, C. Zhen, Y. Tao, R. Chen, H. Shi, T. Chen, Z. Wang, H. Li, R. Deng, X. Liu and W. Huang, *Nat. Mater.*, 2015, **14**, 685–690.
68 A. d. Cózar and C. Romero-Nieto, *Inorg. Chem.*, 2023, **62**(10), 4097–4105.
69 O. Larrañaga, C. Romero-Nieto and A. d. Cózar, *Chem.–Eur. J.*, 2019, **25**, 9035–9044.
70 N. C. Baird, *J. Am. Chem. Soc.*, 1972, **94**, 4941–4948.
71 X. Jin, S. Li, L. Guo, J. Hua, D.-H. Qu, J. Su, Z. Zhang and H. Tian, *J. Am. Chem. Soc.*, 2022, **144**, 4883–4896.
72 Y. Chen, K.-H. Chang, F.-Y. Meng, S. M. Tseng and P.-T. Chou, *Angew. Chem., Int. Ed.*, 2016, **60**, 7205–7212.
73 M. Krug, N. Fröhlich, D. Fehn, A. Vogel, F. Rominger, K. Meyer, T. Clark, M. Kivala and D. M. Guldi, *Angew. Chem., Int. Ed.*, 2021, **60**, 6771–6777.
74 X. Chen, J. Huang, F. Gao and B. Xu, *Chem*, 2023, **9**, 562–575.